DEVELOPMENT OF MINIATURE ROBOTIC ARM MANIPULATORS TO ENABLE SMALLSAT CLUSTERS

BY

THIBAUT WENGER

THESIS

Submitted in partial fulfillment of the requirements
for the degree of Master of Science in Aerospace Engineering
in the Graduate College of the
University of Illinois at Urbana-Champaign, 2017

Urbana, Illinois

Adviser:

Assistant Professor Koki Ho

ABSTRACT

The performances of monolithic spacecraft are limited by their size, mass and cost. For example, the sizes of a communication satellite antenna or of a space telescope primary mirror directly impact their performances. In-space assembly and formation flying missions are the logical responses to this issue. Instead of limited dedicated launches, several small satellites can be piggybacked as secondary payload and work together to accomplish the same mission. Therefore, this concept reduces the cost but also removes the limit of size and mass since more spacecraft can always be added to the formation while increasing robustness (the independent spacecraft are replaceable) and modularity (the reconfiguration of the formation can lead to different outcomes).

This research is the result of a collaboration between the Jet Propulsion Laboratory (JPL) and University of Illinois at Urbana Champaign (UIUC). It presents the development of an integrated, robust and optimized method to enable scalable small satellites clusters via Clusters Forming On-Board Robotic Manipulators (C-FORM). The physical connection removes the constraint of highly sophisticated control for collision avoidance, the main obstacle of formation flying missions. After the deployment phase, pairs of satellites will sequentially rendezvous, deploy their miniature robotic arms and dock with the help of their end effectors. The dockings will be repeated until the formation is formed. JPL developed and designed both the robotic arms and the end effectors. Under the requirements of the mission, the components were selected for the satellite bus. A simulation was developed in order to model the

dynamics of the spacecraft under realistic sensors and actuators to validate the feasibility of this concept. Finally, a quantitative estimation of the amount of fuel the robotic arms can save for formation flying purposes was carried out.

TABLE OF CONTENTS

CHAPTER 1 INTRODUCTION 1

1.1 Description of the concept 1

1.2 Possible applications 3

1.3 Literature review 5

CHAPTER 2 CONCEPT OF OPERATION 9

2.1 Realistic launch scenario 9

2.2 Phases of the mission 10

CHAPTER 3 SATELLITE ARCHITECTURE 12

3.1 Design Requirement 12

3.2 Selected components 13

CHAPTER 4 GUIDANCE NAVIGATION AND CONTROL SYSTEM DESIGN 16

4.1 Objective and assumptions 16

4.2 Control law 18

4.3 Integral Pulse Frequency Modulator 24

CHAPTER 5 SIMULATION RESULTS 32

5.1 Validation of the simulation 32

5.2 Closing approach ΔV and accuracy results 33

5.3 Final approach ΔV and accuracy results 38

CHAPTER 6 BENEFITS OF USING ROBOTIC ARM 41

6.1 Station keeping scenario 41

6.2 Reconfiguration scenario..... 45

CHAPTER 7 CONCLUSION 50

CHAPTER 8 PUBLICATION AND CONFERENCES 52

REFERENCES 53

CHAPTER 1 INTRODUCTION

1.1 Description of the concept

The project of the "Development of miniature robotic arm manipulators to enable smallsat clusters" explores the feasibility of a rendezvous and docking mission between multiple CubeSats using miniature robotic arms to perform the connections between the spacecraft, hold and reconfigure the formation. It is a collaboration between JPL and UIUC. JPL entirely designed and developed the robotic arms and the end effectors. It is a foldable arm with a maximum length of 47 cm, 5 degrees of freedom and a mass of 460 g. Its stowed volume is approximately half a CubeSat unit (10 cm by 10 cm by 5 cm) and its end effector is able to catch the neighbor spacecraft robotic arm almost instantaneously with a force between 20 N and 100 N in a half sphere with a 47 cm radius if the relative positions of the two spacecraft stay within a 10 cm accuracy. This set the constraints of the control design that has been the purpose of this research. Figure 1.1 and Figure 1.2 depict the rendering of the robotic arm and end effector concepts created by JPL:

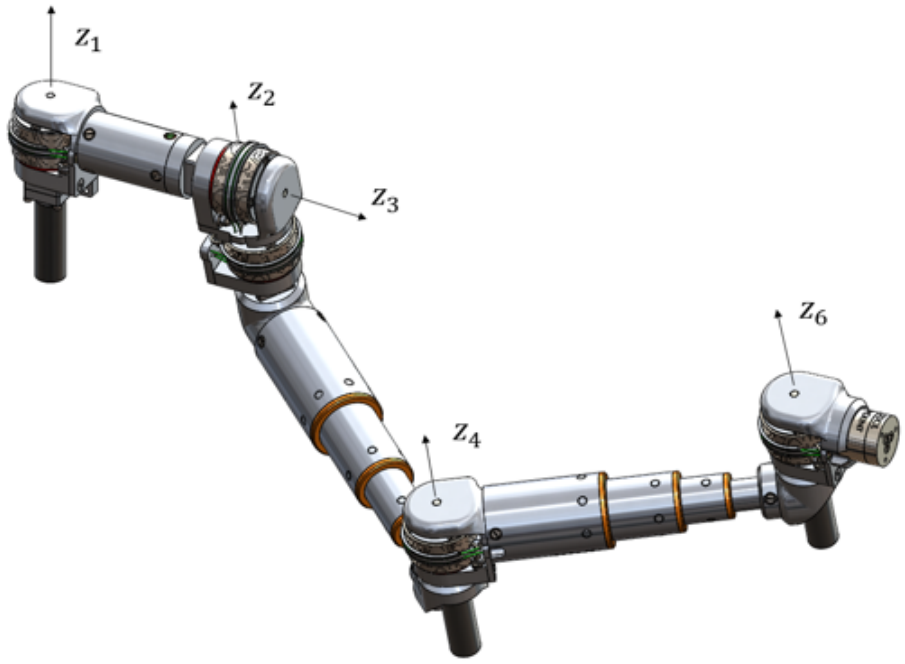

Figure 1.1: Extended robotic arm manipulator, from JPL [1]

Figure 1.2: Rendering of docking end effector, from JPL [1]

This thesis describes the development of the control design of the different satellites. The concept of operations sets the different phases of the rendezvous and docking phases under the constraints risen by a formation flying mission. The components have been selected to form the satellite bus taking into account flight heritage, performances and CubeSat constraints. To assess the feasibility of the mission, a simulation was developed to model the dynamics of a chaser in the vicinity of its target under realistic disturbances and sensor and actuator noises. Finally, the control was derived, which was constrained by the robotic arm requirements, the sensors and actuators selected and the limited fuel available on board.

1.2 Possible applications

The desire for more accurate or powerful space systems requires bigger and more sophisticated satellites, a goal that can only be achieved through in space assembly or formation flying missions due to the limited volume and mass a monolithic satellite can have. This project, introducing C-FORM to enable a SmallSat cluster, is a big step to this end allowing more flexibility and safety for the docking process than an usual structure-to-structure connection. It relaxes the control constraints since the arm is able to move and it increases the separation distances which makes the collision risk lower. The miniaturization of the robotic arm also enables SmallSats to build larger structures in space with a limited number of units. For example, a SmallSat cluster where each

satellite is equipped with a small mirror could assemble in space to build a large telescope with more flexibility in the reconfiguration and less constraints on the control of a large number of spacecraft than any other solutions previously developed. The structures created by these satellites are also scalable, units can easily be removed, added or switched. In this way, new capabilities can be added to existing spacecraft, flawed units can be changed without putting in jeopardy the entire mission and different modes can be reached by changing the formation. For instance, large and scalable antenna or relative repositioning for interferometry missions would directly benefit from these capabilities. This project also introduces a technology demonstration for on orbit servicing that is a way to dramatically increase the lifetime of the satellites in space. A rendering of a SmallSat antenna cluster in Figure 1.3 and a summary of potential applications gathered in Table 1.1 was created by JPL:

Table 1.1: Potential applications to the C-FORM project, from JPL [1]

Construction	Positioning	Reconfigurability	Arm Manipulation
Synthetic aperture radar	Real-time data transmission	Large distributed array (adaptability to different missions)	Large debris tracking and collision avoidance
ISARA reflectarray	Large solar panel pointing	Transfer to and from ISS	Satellite inspection with camera
Optical mirror	Data relay for deep space communications	Replaceable parts to extend mission life	Satellite minor repairs / augmentation
Large Solar Sail	Data relay for far side of moon in L2 halo orbit	New payload modules to expand capabilities of larger satellites	Capture space debris
Altimeter	Interferometry	Steerable radar to cover large swaths	In-orbit assembly

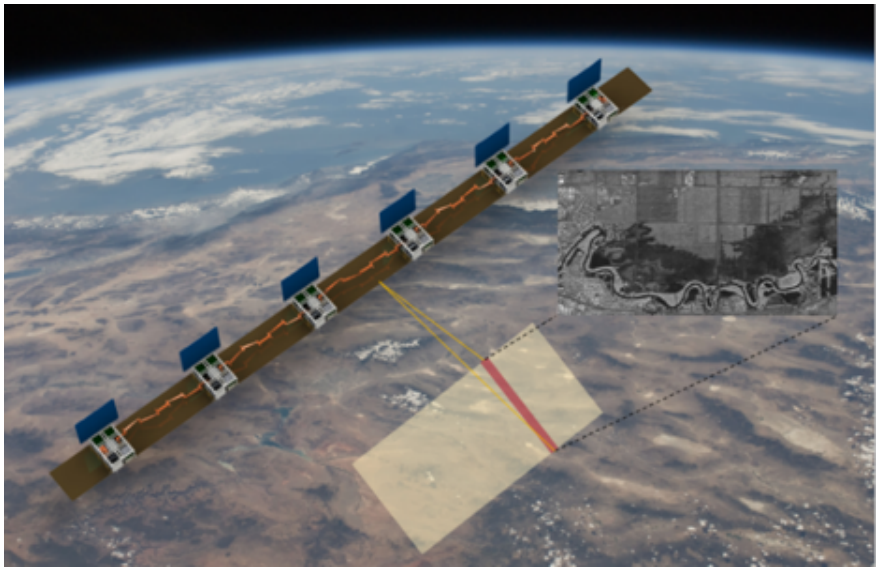

Figure 1.3: Rendering of a SmallSats antenna cluster, from JPL [1]

1.3 Literature review

An extensive literature review was performed in three main areas. The first area of interest is about robotic arms. Previously launched space robotic manipulator technologies have only been large spacecraft with high mass, power, and volume. This research is unique in miniaturizing these robotic arms and using them for docking and relative navigation of multi-spacecraft clusters. Further, some other works detailed different methods for formation flight control that could be applied to the mission. Finally, many space missions have accomplished proximity operations, giving highlights about the sensors and actuators commonly used. They have been gathered

in the Rendezvous, Proximity Operations, Docking and Undocking (RPODU) area. This research belongs to all of these domains.

The idea of using the SmallSat platform to rendezvous and form larger structures is not new. Indeed, there are a few similar concepts currently being explored to advance this idea. The concepts do not, however, employ robotic manipulators but instead focus on linking multiple SmallSat structures to each other.

The first similar concept is called CPOD (SmallSat Proximity Operations Demonstration). This mission, which is currently built and awaiting a flight opportunity, will launch two 3U SmallSats linked together from the same P-Pod deployer. They will then detach and perform proximity operations, flying around each other multiple times to image the other craft. Finally, the two units will autonomously dock [2]. The CPOD mission serves as an excellent technology demonstration for the C-FORM concept presented here as it will demonstrate close proximity operations and autonomous docking of two SmallSats which will be necessary in linking the robotic manipulators to each other.

The second mission currently exploring SmallSat rendezvous concepts is AAReST (Autonomous Assembly of a Reconfigurable Space Telescope). This concept comes from Caltech and proposes a 27U SmallSat that will be deployed as one unit. Once on orbit the system will detach two 3U units that will then use a propulsion system to move to a new position on the large craft and dock. This is meant to demonstrate the ability to reconfigure the entire system to construct different types of space telescopes [3]. AAReST provides an excellent technology demonstration of a reconfigurable

system that will prove useful when exploring potential payloads and concepts for the C-FORM platform.

Another challenge raised by a formation flying mission involves the specific optimal control governing the motion of the satellites in a cluster. Hamel addressed this issue and stated the three main trades related to this topic: fuel consumption, collision avoidance and formation lifetime [4]. Several theories were then presented with their assumptions, advantages and limitations. The most commonly used are the linear Clohessy-Wiltshire (CW) equations to represent the dynamics of a chaser in the frame of the target satellite. The simplicity of this model allows the derivation of straightforward command laws [5-6]. However, as outlined by Hamel, this model is also restrictive since it assumes a circular non-perturbed orbit with cooperative satellites. More complicated studies investigated a nonlinear approach taking into accounts disturbances, elliptical orbits or non-cooperative target (i.e. the motion of the target is not completely known) [6-8]. Lastly, in order to increase the robustness and reduce the computation cost of the algorithm, Morgan et al. proposed a method to decentralize the computations [9]. Each satellite calculates its optimized trajectory and only takes into account the neighboring spacecraft. Morgan et al. used Sequential Convex Programming (SCP) and Model Predictive Control (MPC) to update the optimal trajectory during the reconfiguration computationally efficiently.

Existing relative navigation and propulsion systems for spacecraft include the differential GPS (DGPS), RF method (e.g., radar), and optical method (e.g., camera, laser) [10-11]. Most of these technologies have not been compatible with SmallSat size or power requirement [12-16]. However, some missions already started to look into the

feasibility to equip SmallSats to perform rendezvous using miniaturized sensors and actuators [17-18]. DGPS has been applied on SmallSats CanX-4 and CanX-5 in 2014 [19], which was claimed as the first formation flying SmallSat cluster, and on the two RAX missions [20]. However, DGPS has limitations in its limited operating altitude and its inability to determine the relative attitude of each small spacecraft.

As opposed to the traditional approach in spacecraft relative control, the proposed concepts use the physically connected robotic arm for relative navigation of the spacecraft. This system can operate at any altitude, and determine the relative position and attitude of the spacecraft altogether, which introduces the system simplicity. Also, the rigid connection of the spacecraft using a robotic manipulator removes the challenges caused by relative drift in the conventional relative navigation and control system. Finally, we can also remove the risks of the collision and signal interference, both of which are serious problems in conventional formation flying spacecraft clusters.

CHAPTER 2 CONCEPT OF OPERATION

2.1 Realistic launch scenario

As a low cost launch solution, the satellites will be integrated with the other payload and brought to the ISS in a dragon spacecraft used to deliver cargo to the station. These SmallSats will be deployed by the NanoRacks CubeSat Deployer, which has the proven flight heritage for launching small satellites. It can carry up to eight 6U CubeSats (in 1x6 or 2x3 configurations) and launch them in the same orbit. The direction of the initial delta V provided by the NanoRacks CubeSat Deployer will be chosen in order to avoid any interference with the ISS orbit. The main advantage of this method includes ability to control time spent between each launch and in turn adjusting the separation distance between each satellite in the initial distribution of the SmallSat. At the end of the launch phase, each satellite will be stabilized on the same circular orbit with a separation distance of five kilometers between them. Each satellite will spend about 1 m/s delta V (the same as the one initially provided by the NanoRacks CubeSat Deployer) to reach the target circular orbit with about 400km altitude and 51.6° inclination.

2.2 Phases of the mission

After this preliminary launch and deployment phase, the SmallSats cluster will be on the same circular orbit with a separation distance of 5 km between each satellite. The target will be chosen as one of the satellite in the middle of the formation. The significant distances between the spacecraft allow us to consider a one chaser – one target scenario for each rendezvous and docking sequence, which removes the high computation constraint raised by the control of a satellite cluster increasing exponentially with the number of spacecraft. In each sequence, the closest chaser will move to dock with the target, creating the new target for the following sequence. The next closest chaser will then move to dock to join the two previous spacecraft. This sequence will repeat until all the satellites of the cluster are successfully docked between each other. Each sequence will be defined in 3 phases. The first phase is a safe closing approach to bring the chaser from few kilometers to 100 meters from the target in the velocity direction using the GPS sensors. In the following phase, the chaser will move from 100 meters to 4 meters from the target using GPS sensors, still in the velocity direction in order to reach the proximity sensors range and prepare the third and final approach. This last phase will see the chaser coming from 4 meters to 60 centimeters from the target using its high accuracy proximity sensors for precise maneuvers. Finally, it will hold this position at a 1 centimeters accuracy in order for the satellites to deploy their robotic arms and dock. Note that only the first phase will change according to the chaser since the initial distances will be multiple of 5

kilometers for subsequent chasers. The increments in separation distances will have a minimal effect on delta V while satisfying the fuel margin. The concept of operation of the first sequence is described in the following Figure 2.1, once the two satellites docked the next sequence follows the exact same phases with the new target being the union of the two first satellites.

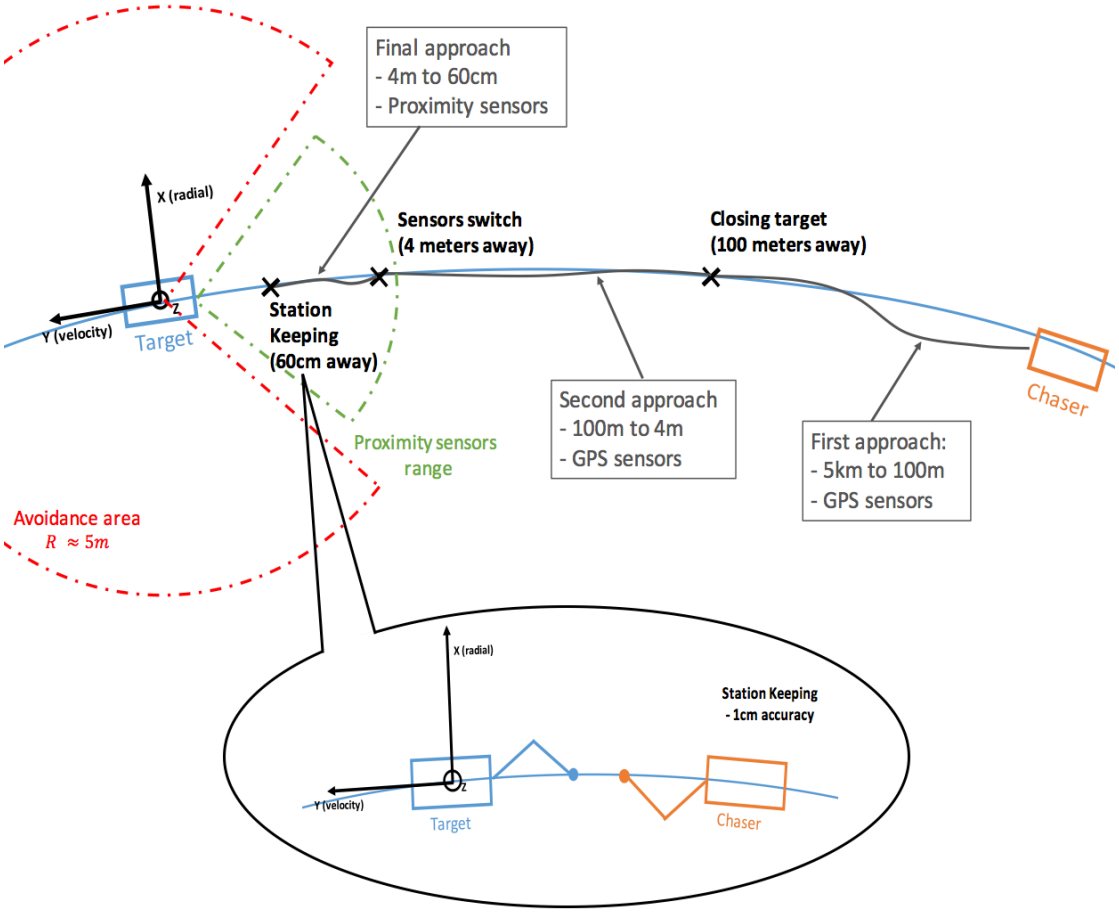

Figure 2.1: Concept of operation of a representative rendezvous and docking sequence with the circular target reference orbit in blue

CHAPTER 3 SATELLITE ARCHITECTURE

3.1 Design Requirement

The concept explored requires the spacecraft to perform rendezvous and proximity operations where the accuracy to achieve docking with the help of the robotic arms. The satellite needs to be equipped with precise absolute and relative position sensors for the closing phases and final approaches. The thruster system has to be capable of providing a delta-V large enough to gather the satellites together and has to be precise enough to enable a safe final approach in compliance with the robotic arm constraints. The attitude and determination control also needs to provide a high attitude pointing and determination accuracy in order to perform the docking. Since the mission is designed to last a few years, the on board computer has to be both robust to the harsh conditions in the space environment and powerful to compute the necessary maneuvers for rendezvous and proximity operations. Omnidirectional uplink communication antennas are also required to handle situations when no ground station is in viewed. Finally, the bus will need to have a power system designed to provide the required power for all the other subsystems and the payload, batteries will be included to provide electricity when the satellites do not face the Sun. The selection of the components briefly described in the next sections was based on these requirements to create the satellite bus. Flight heritage has been prioritized as much as possible.

3.2 Selected components

GPS sensors are required for the absolute position determination of the satellites during their mission. As they will also be used for the relative navigation solution for the two first phases of the mission, a high accuracy is required. The NovAtel OEM615 Dual-Frequency GPS [21], flight proven by GomSpace is a dual frequency receiver providing a 1.5 m accuracy, which is enough for the two first closing approaches before the spacecraft can switch to the more accurate proximity sensors. Indeed, for the final approach a better accuracy is required. The simulation was based on the SoftKinetic DS525 sensor [22]. It has a 4 m range, which constrained the second phase of the mission and a 14 mm accuracy, enough to satisfy the relative position requirements of the robotic arm for the final docking phase. It is a miniaturized and more performant version of the SoftKinetic sensor that has been used by the AAReST mission which will need to be adapted for space use (a high contingency has been applied for its impact on the mass budget).

The thruster system selected is the Vacco Reaction Control Propulsion Module [23]. It can provide a 15 m/s delta V for a 12 kg satellite which leaves a comfortable margin since the rendezvous operations require less than 5 m/s delta V. Its main advantage relies on its 8 thrusters design which enables the spacecraft to thrust in any desired direction at anytime. It is based on a cold gas propellant technology which has a good

flight heritage. Finally, its low minimum impulse bite of 0.2 mNs allows for precise maneuvers during the final approach that satisfy the end effector requirements.

The Attitude Determination and Control System (ADCS) chosen is the Blue Canyon Technology XACT [24]. It has been selected for its compactness and light weight (0.5 CubeSat unit and 910 g). It is a complete ADCS solution including star tracker, sun sensors, three reaction wheels, three torque rods, IMU and magnetometer for a 0.007 deg three axis pointing accuracy with a minimum slew rate of 10 deg/s for a 4kg 3U CubeSat.

The On Board Computer (OBC) selected is the 10 MHz Space Micro Proton Proton200k Lite [25]. It is space qualified for a mission lifetime of at least three years at Low Earth Orbit. Its storage capabilities of 32 GB of flash memory and 512 Mo of RAM will allow to support the Guidance, Navigation and Control software in addition to the science data prior to their downlink back down to a ground station on Earth.

The communication system was designed in order to allow the spacecraft to communicate with the ground stations while keeping any attitude required by science operations or rendezvous purposes. A UHV/VHF system by Innovative Solution in Space [26] provides the omnidirectional antenna required with a 1.2 kbps uplink and 9.6 kbps downlink transfer rates. Another antenna designed by Endurosat [27] can be used in the S-Band while facing a ground station for a better transfer rate of 100 kbps once the science operation is done.

Finally, the power system was selected to generate electricity through solar panels, distribute this power to the subsystems and store energy to support operations when the spacecraft does not view the Sun. Clyde Space provides solar panels for CubeSats that

generate 7 W for three CubeSat units. Their power distribution subsystem is designed to handle space radiations and the storage capacities of the batteries goes up to 40 Wh [28].

CHAPTER 4 GUIDANCE NAVIGATION AND CONTROL SYSTEM DESIGN

4.1 Objective and assumptions

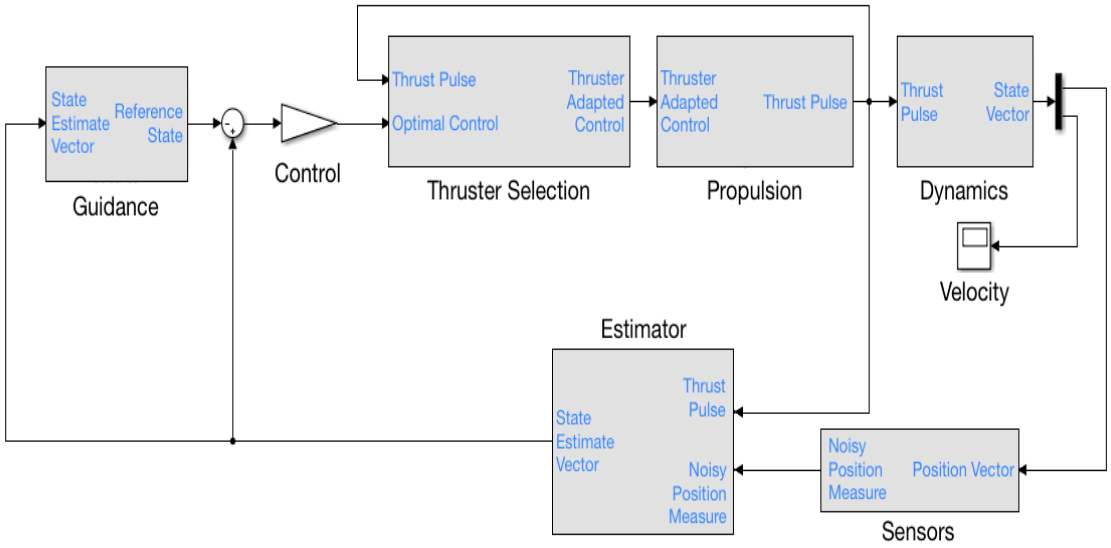

Figure 4.1: Architecture of the GNC system design

As stated in the concept of operation, the SmallSat cluster formation will start from a distributed configuration with around 5 km separation distance between each satellite right after the deployment. They will reach their final configuration by sequentially docking with each other with the help of robotic arms. Each sequence will consist of bringing one chaser from few kilometers to few centimeters apart from the target with a 10 cm accuracy. The objective of the Guidance, Navigation and Control system is to develop and optimize an integrated control method to bring each chaser sufficiently

close to its target in order to deploy its robotic arm and dock. The constraints of the design include the mass, size, power and volume of each SmallSat.

The architecture of the feedback Guidance Navigation and Control system is illustrated in Figure 4.1. It is broken down into 7 major parts:

- The “Guidance” block computes the reference signal according to the current state of the satellite. Different modes with different targets to reach are initiated by the position and velocity information feeding the guidance block. The different references along the rendezvous sequence are in compliance with the phases of the mission described in Chapter 3.
- The “Control” block is responsible for driving the error signal (current state – reference state) to 0 by computing the optimal control to apply. It will also directly impact the performance of the system (accuracy, stability, time to converge, fuel consumption). Its derivation will be detailed later.
- The “Thruster Selection” block translates the continuous control computed by the “Control” block to discrete pulses achievable by the thrusters. Its purpose is to select the optimum thrust to apply in order to appropriately implement the continuous optimal control input. Its functioning will be explained later.
- The “Propulsion” block models the real actuators of the spacecraft. Angle and thrust magnitude errors are modeled by random white noise. Minimum

impulse time is modeled with a hold block that keeps the signal constant during this time.

- The “Dynamics” block models the relative equations of motion of the spacecraft. It includes the J2 effect and the relative drag, which are the two main relative disturbances acting on the satellites.
- The “Sensor” block models the GPS/proximity sensors, adding a random white noise to the real position input.
- The “Estimator” block is a Kalman filter that provides the best estimation of the current state from the observations input given by the GPS/proximity sensors.

As a fully representative step to this end, this section looks into the rendezvous and docking of one SmallSat to another under realistic noises and errors of its sensors and actuators. The dynamics of the chaser will also be subjected to relative J2 and atmospheric drags, which are the two dominant disturbances in this scenario.

4.2 Control law

For the selected relative motion control design, several assumptions were considered to simplify the model. As described in Chapter 2, in regards to the initial configuration of the cluster, all the satellites will be in the same circular orbit, separated by 5 km

along the direction of the motion. Therefore, the target spacecraft was considered to be in a circular orbit that defined the reference frame as depicted in Figure 4.2:

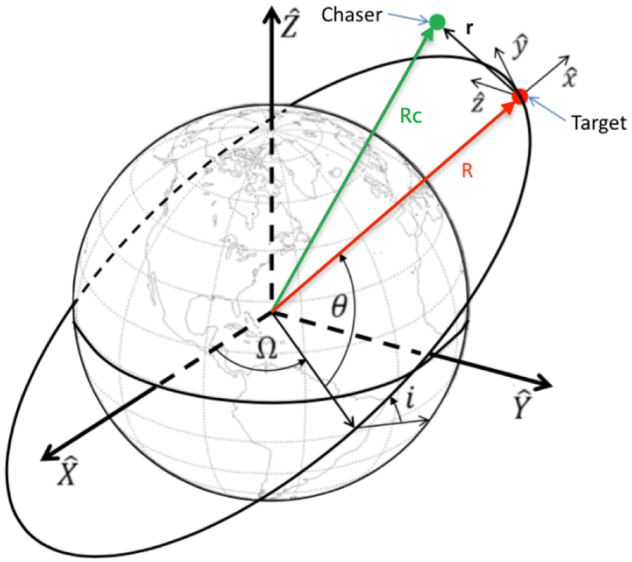

Figure 4.2: Reference orbit of the target and reference frame, adapted from [9]

Here, X-axis is along the radius vector of the target spacecraft, Y-axis is along the velocity of the target spacecraft, Z-axis completes the right handed system. In the global frame, the dynamics of the target (reference) and chaser follow the equations:

$$\ddot{\boldsymbol{R}} = -\mu \frac{\boldsymbol{R}}{|\boldsymbol{R}|^3} + \boldsymbol{d_t} + \boldsymbol{u_t} \tag{4.1}$$

$$\ddot{\boldsymbol{R}}_{\boldsymbol{c}} = \ddot{\boldsymbol{R}} + \ddot{\boldsymbol{r}} = -\mu \frac{\boldsymbol{R} + \boldsymbol{r}}{|\boldsymbol{R} + \boldsymbol{r}|^3} + \boldsymbol{d_c} + \boldsymbol{u_c} \tag{4.2}$$

Where $\boldsymbol{d_c}$, $\boldsymbol{d_t}$, $\boldsymbol{u_c}$ and $\boldsymbol{u_t}$ are respectively the chaser and target disturbances and chaser and target control accelerations and μ is the gravitational parameter of the Earth. For relative control and rendezvous operations it is much more convenient to work in the frame defined by the target. Subtracting Equation 4.1 to Equation 4.2 leads to the relative dynamics of the chaser with respect to its target:

$$\ddot{\boldsymbol{r}} = -\mu\left(\frac{\boldsymbol{R}+\boldsymbol{r}}{|\boldsymbol{R}+\boldsymbol{r}|^3} - \frac{\boldsymbol{R}}{|\boldsymbol{R}|^3}\right) + (\boldsymbol{d_c} - \boldsymbol{d_t}) + (\boldsymbol{u_c} - \boldsymbol{u_t}) \tag{4.3}$$

Considering that the target is only passively cooperative (i.e. its shape and orbital parameters are known but it is not controlled), we can define the relative control as $\boldsymbol{u} = \boldsymbol{u_c} - \boldsymbol{u_t} = \boldsymbol{u_c}$. The relative disturbance (J2 and Drag) modeled by the dynamics block is noted $\boldsymbol{d} = \boldsymbol{d_c} - \boldsymbol{d_t}$. Projecting Equation 4.3 in each of the vector component directions of $\boldsymbol{r} = [x\ y\ z]^T$ in the relative frame defined in Figure 4.2 leads to:

$$\ddot{x} = 2n\dot{y} + n^2(|\boldsymbol{R}| + x) - \frac{\mu}{|\boldsymbol{R_c}|^3}(|\boldsymbol{R}| + x) + d_x + u_x \tag{4.4}$$

$$\ddot{y} = -2n\dot{x} + n^2 y - \frac{\mu}{|\boldsymbol{R_c}|^3} y + d_y + u_y \tag{4.5}$$

$$\ddot{z} = -\frac{\mu}{|\boldsymbol{R_c}|^3} z + d_z + u_z \tag{4.6}$$

With $n = \sqrt{\frac{\mu}{R^3}}$ the constant orbital rate of the target in its circular orbit. Furthermore, since $|\boldsymbol{R}| \gg |\boldsymbol{r}|$, the first order Taylor expansion:

$$\frac{1}{|\boldsymbol{R_c}|^3} = ((|\boldsymbol{R}| + x)^2 + y^2 + z^2)^{-3/2} \approx \frac{n^2}{\mu}(1 - 3\frac{x}{|\boldsymbol{R}|}) \tag{4.7}$$

can accurately lead to the well-known Clohessy-Wiltshire equations:

$$\ddot{x} = 3n^2x + 2n\dot{y} + u_x + d_x \tag{4.8}$$

$$\ddot{y} = -2n\dot{x} + u_y + d_y \tag{4.9}$$

$$\ddot{z} = -n^2z + u_z + d_z \tag{4.10}$$

Additionally, we assume the presence of sensor noise and actuator uncertainties in the model. These are modeled through Gaussian white noise with realistic power spectral density from the datasheets. Also, no attitude control is considered in this preliminary relative control design. Finally, the mass loss due to the propellant consumption is not considered since it is insignificant. Added to the circular orbit assumption (constant n), this set of linearized equations (Equation 4.8, Equation 4.9 and Equation 4.10) can be expressed in a state-space system, giving rise to a constant A matrix:

$$\dot{\boldsymbol{x}} = A\boldsymbol{x} + B\boldsymbol{u} + \boldsymbol{v} \tag{4.11}$$

$$\boldsymbol{y} = C\boldsymbol{x} + \boldsymbol{w} \tag{4.12}$$

$$\boldsymbol{x} = \begin{bmatrix} x \\ y \\ z \\ \dot{x} \\ \dot{y} \\ \dot{z} \end{bmatrix} \tag{4.13}$$

$$A = \begin{bmatrix} 0 & 0 & 0 & 1 & 0 & 0 \\ 0 & 0 & 0 & 0 & 1 & 0 \\ 0 & 0 & 0 & 0 & 0 & 1 \\ 3n^2 & 0 & 0 & 0 & 2n & 0 \\ 0 & 0 & 0 & -2n & 0 & 0 \\ 0 & 0 & -n^2 & 0 & 0 & 0 \end{bmatrix} \tag{4.14}$$

$$B = \begin{bmatrix} 0 & 0 & 0 \\ 0 & 0 & 0 \\ 0 & 0 & 0 \\ \frac{1}{m} & 0 & 0 \\ 0 & \frac{1}{m} & 0 \\ 0 & 0 & \frac{1}{m} \end{bmatrix} \tag{4.15}$$

$$C = \begin{bmatrix} 1 & 0 & 0 & 0 & 0 & 0 \\ 0 & 1 & 0 & 0 & 0 & 0 \\ 0 & 0 & 1 & 0 & 0 & 0 \end{bmatrix} \tag{4.16}$$

where $\boldsymbol{x}$ is the vector of state variables of the system (i.e., relative position and velocity of the chaser), $\boldsymbol{u}$ is the vector of control inputs (i.e., thrust), and $\boldsymbol{y}$ is the vector of the outputs available for feedback (i.e., position feedback). $\boldsymbol{v}$ and $\boldsymbol{w}$ are respectively the system actuator noise and sensor noise. Also, m is the spacecraft mass.

The thrust is computed with a feedback control law: $\boldsymbol{u} = -K\boldsymbol{x}$, where the gain K is optimized by solving the Linear-quadratic Gaussian (LQG) problem. The LQG control is created in the Simulink model with realistic SmallSat sensor and actuator noises and errors based on the datasheets of the selected hardware. LQG is a combination of Kalman filter and Linear-quadratic regulator (LQR) and gives a robust optimal control law to the linear system under actuator/sensor noises. The cost function of the optimal control law is a tradeoff between the convergence speed and the control effort as follows:

$$\mathrm{J} = \mathrm{E}\left[\int_0^T \boldsymbol{x}^T Q\boldsymbol{x} + \boldsymbol{u}^T R\boldsymbol{u}\, dt\right] \tag{4.17}$$

In the cost function, E[·] stands for expected value over the sensor and actuator noises while the cost of deviation from the target state and control input are respectively penalized by the matrices Q and R. In the nominal analysis, we consider the weighting of Q to be a diagonal matrix with the top three elements to be n^2 and bottom three each equaling to 50. The matrix R is set to $10/n^2 I_3$ with I_3 being the identity matrix in $\mathbb{R}^3$. Larger numbers in this matrix represent the importance in the saving fuel during the rendezvous process. The diagram of the resulting Simulink model is shown in Figure 4.1.

4.3 Integral Pulse Frequency Modulator

The main limitation of the chemical thrusters onboard the spacecraft is that they can only provide discrete pulses of thrust, while the optimal control computed by the LQG controller is continuous. The latter has been derived in order to find the best performance according to the constraints of the problem but the overall performance of the real system will depend on the ability of the thruster impulses to follow this optimal command. Setting a threshold defining whether or not the thrusters should be activated is not sufficient to address this issue:

- If the threshold is too high, the accuracy will be lowered. Since the control is proportional to the error signal feeding the controller, when the spacecraft is too close to its current target, the control will be under the threshold and the thrusters will stop even if the error is not zero.
- If the threshold is too low, the system will be very sensitive to noise. The thrusters will be activated too frequently, even when the input control is just the result of the difference between the estimate and real states. This will lead to an increase in the fuel spent.

Both ways have drawbacks that are lowering the performance of the optimized control method and neither of them is able to accurately follow the control input derived by the optimization process. Moreover, since the optimization statement does not take into

account of this limitation, the optimized metric (time to converge and fuel spent) is not directly linked to the simulation results.

Therefore, in order to appropriately trigger the 25mN thrusters, a pulse modulator strategy is used. A pulse modulator modulates the pulse output of the thruster according to the continuous input of the controller.

This strategy is commonly used in control design to solve the continuous control/discrete pulse issue raised above. The CanX-4&5 mission which aims at performing formation flying mission between two nanosatellites implemented a Pulse Width Modulation (PWM) strategy [2]. At every PWM cycle, the modulation aims at varying the length of the thruster on time according to the control input magnitude at the beginning of this cycle. This strategy has been elaborated in order to address their thruster constraint: their satellite is equipped with only one thruster; they therefore need a long time (included in the PWM cycle time) to change the attitude of the spacecraft to thrust in the required direction.

For a satellite with 6 thrust directions available, a better strategy can be implemented. An Integral Pulse Frequency Modulator has been chosen as the one described in [29]. The purpose is to thrust during the minimum impulse time achievable by the thruster (0.08s) and modulate the thrust frequency according to the control input. The smaller time sample makes the thrust output better follow the optimized control input. Since the modulator compares the integral of the two signals, it works with the control and thruster impulses. It enables the propulsion system to get rid of the random command

noise, which gets canceled through the integration process and leads to propellant saving.

Thus, at any time t_k, the objective is to minimize the impulse error:

$$\boldsymbol{J_k} = \int_0^{t_k} (\boldsymbol{u}(t) - \boldsymbol{T}(t))dt \tag{4.18}$$

With $\boldsymbol{u}$ being the continuous optimized control input, $\boldsymbol{T}$ being the discrete pulse output and $t_k = k\Delta t$ being the current sample time where Δt is the minimum impulse time of the thrusters. Subsequently, the next pulse is determined according to the following law:

$$Between\ t_k\ and\ t_{k+1},\ T_i(t) = \begin{cases} T & if\ \ J_{k,i} \geq T\Delta t \\ 0 & if\ \ J_{k,i} < T\Delta t \end{cases} where\ i = x, y, z \tag{4.19}$$

As a consequence, the impulse error grows as the control is accumulating through the integration and is set to zero every time it reaches the minimum impulse achievable by the thrusters. If the control input is only due to noise because of the satellite already close to its target, the integration of the signal is zero and the thrusters are not activated. Figure 4.3 and Figure 4.4 show an example of an optimal control input and its pulse output profile when a chaser is reaching its target from 5 km to 0 km:

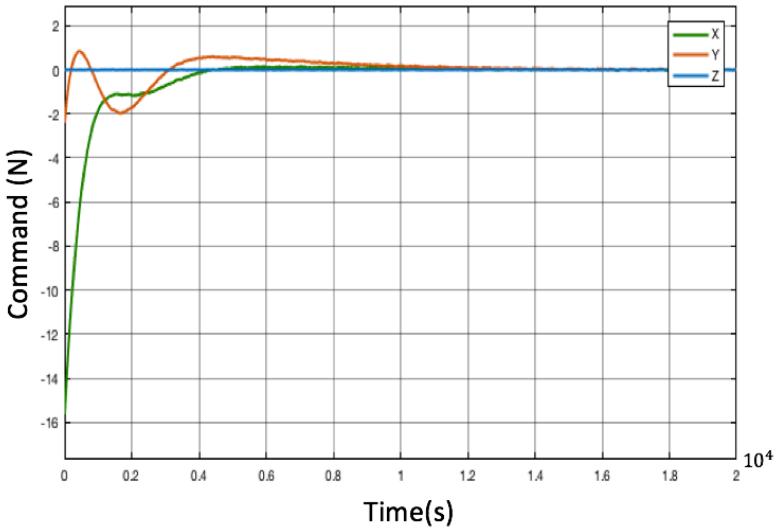

Figure 4.3: Optimal continuous command acceleration computed over time for a chaser going from 5 km to 0 km

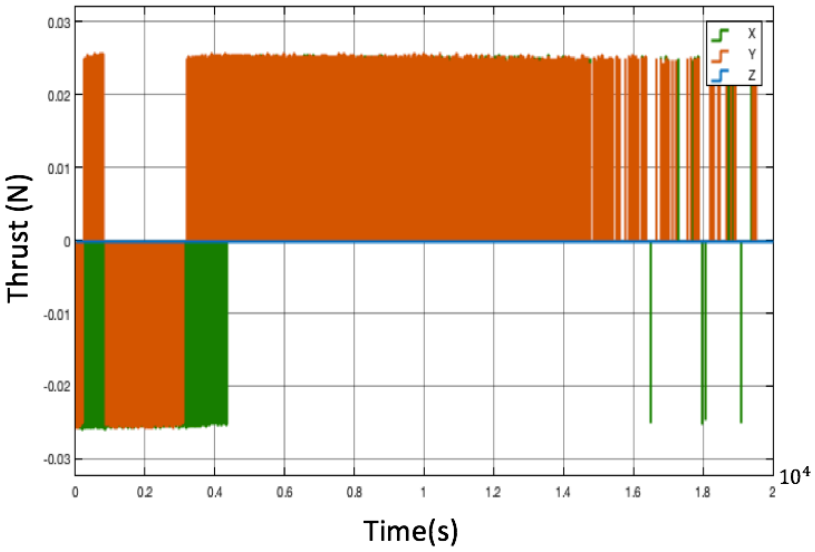

Figure 4.4: Corresponding thrust profile output computed over time for a chaser going from 5 km to 0 km

Figure 4.5 and Figure 4.6 show how the optimized impulse control is approximated by the Integral Pulse Frequency Modulator thruster impulse for the exact same mission:

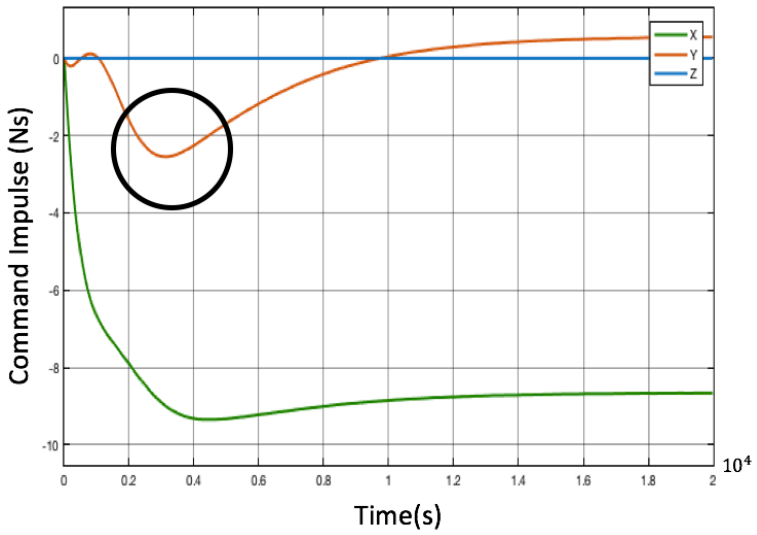

Figure 4.5: Optimal continuous command impulse computed over time for a chaser going from 5 km to 0 km, the circle area is zoomed in Figure 4.7

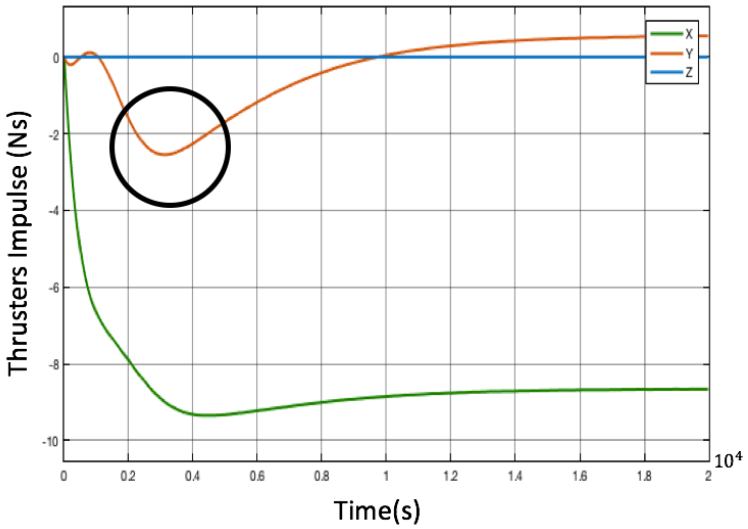

Figure 4.6: Corresponding thrust impulse output computed over time for a chaser going from 5 km to 0 km, the circle area is zoomed in Figure 4.8

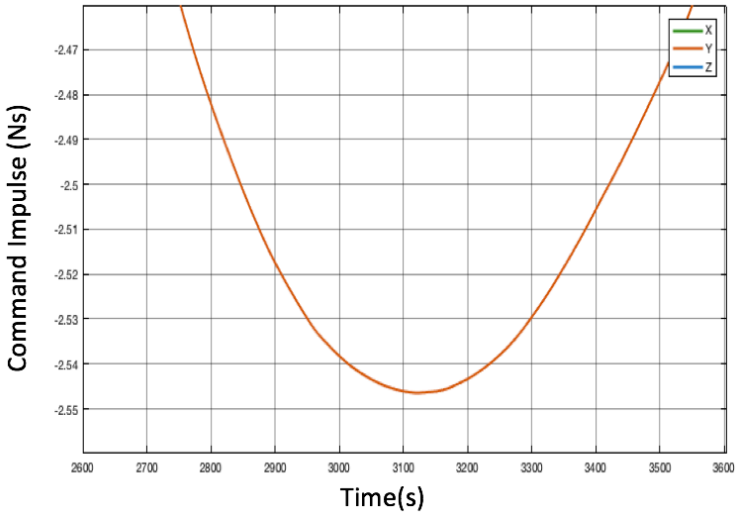

Figure 4.7: Zoom from Figure 4.5 on the optimal continuous command impulse computed over time for a chaser going from 5 km to 0 km

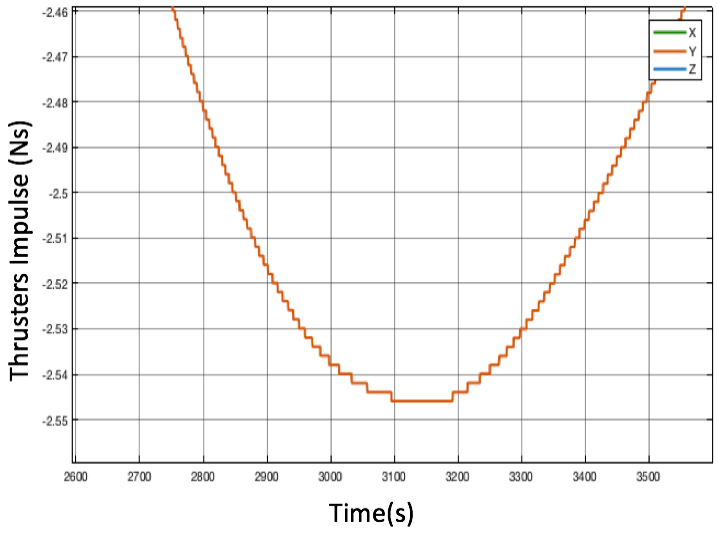

Figure 4.8: Zoom from Figure 4.6 on the corresponding thrust impulse output computed over time for a chaser going from 5 km to 0 km

Figures 4.7 and Figure 4.8 clearly show how the Integral Pulse Frequency Modulator approximates the continuous optimal input computed by the LQG corrector. Each step

corresponds to the minimum impulse achievable by the thrusters, which therefore directly impacts the ability of the satellite to follow the optimized command law. The impulse error, the difference between the command impulse and the thrusters' impulse, is shown in Figure 4.9. The minimum impulse bite of the thrusters corresponds to the maximum impulse error the spacecraft can accumulate until it thrusts:

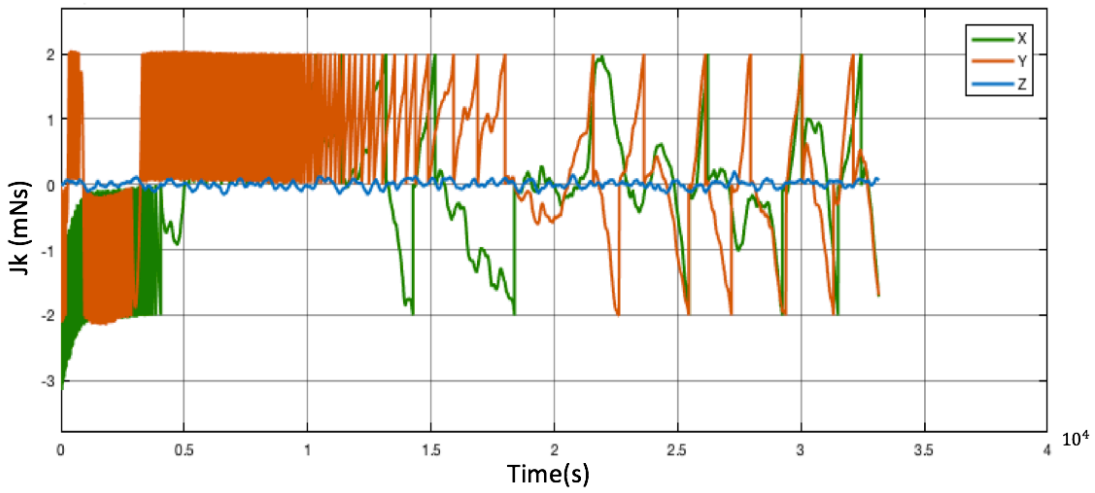

Figure 4.9: Impulse error over time, the minimum impulse is 2mNs here (25 mN thrust, 0.08 s minimum impulse time), we see that through the integration, the noise of the Z axis does not impact the thrusters

The gain also has to be adapted according to the characteristics of the real thrusters and sensors since it is based on the feedback law $\boldsymbol{u} = -K\boldsymbol{x}$. Indeed, in order to keep the error as low as possible (which means that the thrusters follow the optimized command better), an impulse from the thrusters should bring the impulse error closer to 0. If the gain is too high and the thrusters are too weak to follow the input command, the error will grow over time, which could result in instability, high amount of fuel wasted and

inaccuracy. In the other hand, since $\boldsymbol{u} = -K\boldsymbol{x} = -K(\boldsymbol{x}_{real} + \boldsymbol{x}_{noise})$, if the minimum impulse is too low as compared to the corresponding sensors accuracy, the thrusters could be triggered because of noise, resulting in fuel spent increase. From a control point of view, it is useless for the spacecraft to have a really low minimum impulse bite if the accuracy of its sensors is not good enough and reciprocally. Therefore, the gain has been adapted during the three phases of the mission in order to increase the accuracy as long as the chaser comes closer to the target. To this effect, the frequency of the Integral Pulse Frequency Modulator has also been adapted to the sensors used: from 0.08 s with GPS to the minimum impulse time 8 ms with the proximity sensors.

CHAPTER 5 SIMULATION RESULTS

5.1 Validation of the simulation

The main purpose of this simulation is to model the dynamics of a chaser in the vicinity of its target spacecraft with realistic sensors and actuators in order to determine the feasibility of the robotic arm formation flying mission. Before exploiting the results for our specific problem, a validation simulation has been carried out based on the literature in this field. As described by H. Djojodihardjo in [30], it can be easily found that for the Clohessy-Wiltshire equations, in the absence of control or external disturbances, the bounded trajectory of the chaser describes an ellipse around its target:

$$x(t) = A_0 \sin(\omega t + \alpha) \tag{5.1}$$

$$y(t) = 2A_0 \cos(\omega t + \alpha) + C_0 \tag{5.2}$$

$$z(t) = B_0 \sin(\omega t + \alpha) \tag{5.3}$$

Where A_0, B_0, C_0 and α are defined by the initial conditions. Without disturbances, these trajectories are perfectly replicated by the simulation, which shows the accuracy of the considered linearized model for a chaser in the vicinity of its target.

The PRISMA project, which successfully accomplished its mission in 2010 and showed proximity operations between two satellites, shares similarities with this presented concept. In their station keeping operation at +-60 meters (along the velocity direction) accuracy, the PRISMA mission simulation [31] reported a daily total delta V spent was 0.0372m/s. Using the different characteristics of their spacecraft (mass, size, actuators, sensors, orbit, …) the presented simulation and control method showed a comparable daily fuel spending.

5.2 Closing approach ΔV and accuracy results

A preliminary simulation computed the rendezvous between two 12 kg SmallSats in a LEO circular orbit at an altitude of 400 km. They start at a 5 km separation distance on the same circular orbit before the chaser activated its thrusters to reach the target satellite. Based on the literature review of the actuator and component datasheets selected to form this SmallSats bus, a realistic model has been realized. For sensors, we consider GPS sensors (noise standard deviation 1.5 m) and proximity sensors (noise standard deviation 14 mm; maximum range 4 m). For actuators, cold gas thrusters have been selected (25 mN +- 5 mN nominal thrust; minimum impulse 0.2mNs; Isp 40 s) as they provide a 6 degrees of freedom thrust with a total delta V of 15 m/s, which has been proven to be enough to accomplish the mission. For our purpose, the accuracy of the GPS sensor is not sufficient but the range of the high accuracy proximity sensor is

too short; therefore, we consider a multi-phase concept: to use the GPS sensor to bring the chaser from 5 km apart to few meters apart (phase 1 and 2), and then use the proximity sensors to navigate the remaining distance (phase 3).

In the above described phases, the satellite moves from about a 5 km distance to 100 m to 4 m (on the y axis) using GPS sensors. The starting point is at [-5 km; 0 km; 0 km]. The resulting X, Y relative position of the chaser is shown in Figure 5.1, Figure 5.2, Figure 5.4 and Figure 5.5. The delta-V over time is shown in Figure 5.3 and Figure 5.6. The transition from phase 1 to phase 2 is determined by the guidance system when the intermediary target is reached.

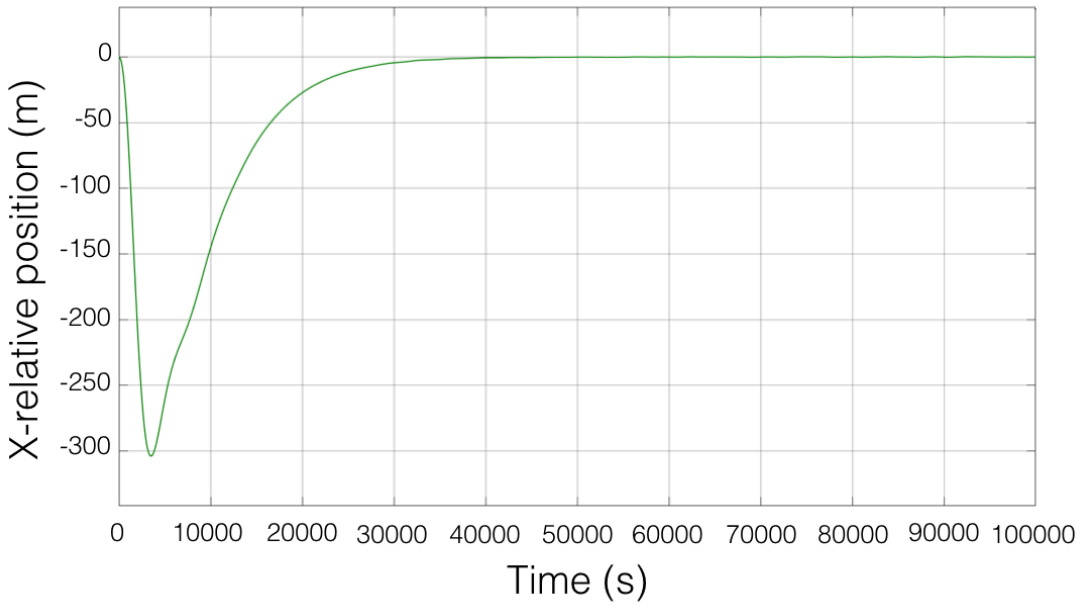

Figure 5.1: X-relative position over time using the GPS for the first closing approach

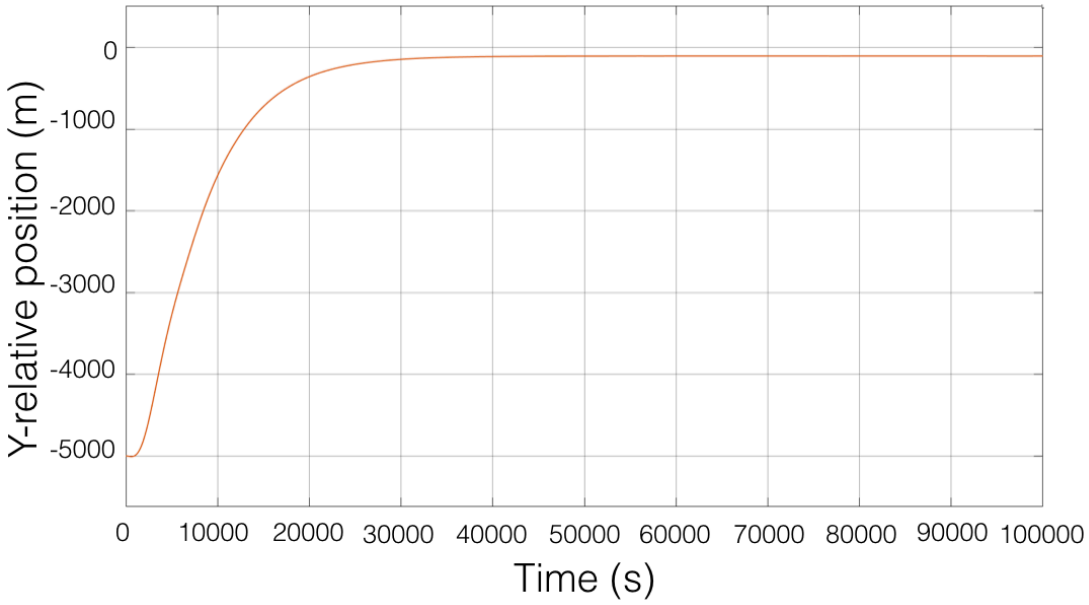

Figure 5.2: Y-relative position over time using the GPS for the first closing approach

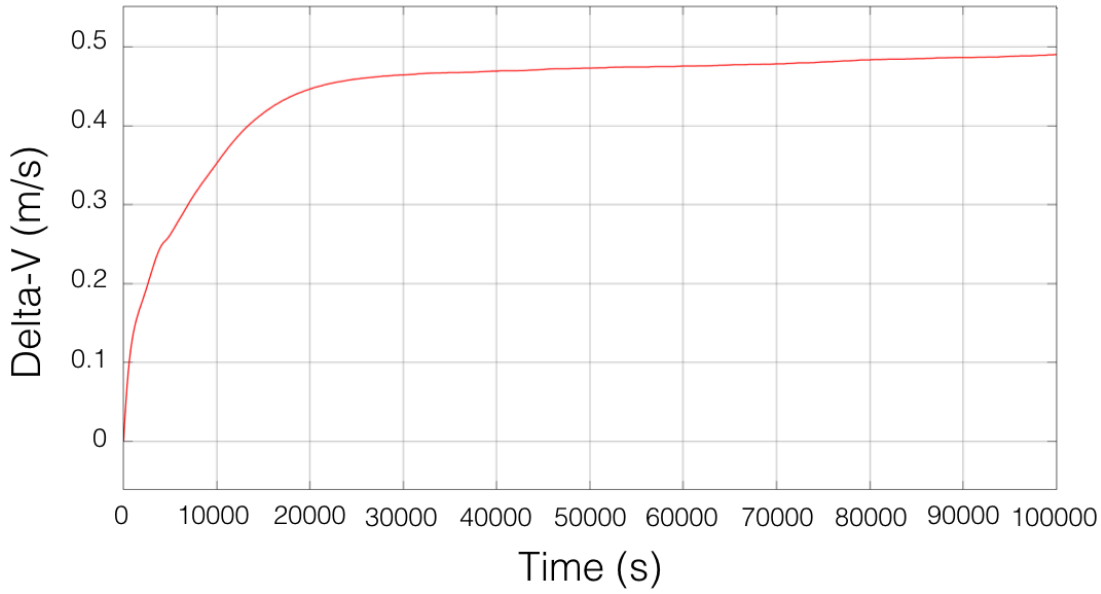

Figure 5.3: Delta-V spent during the first closing approach

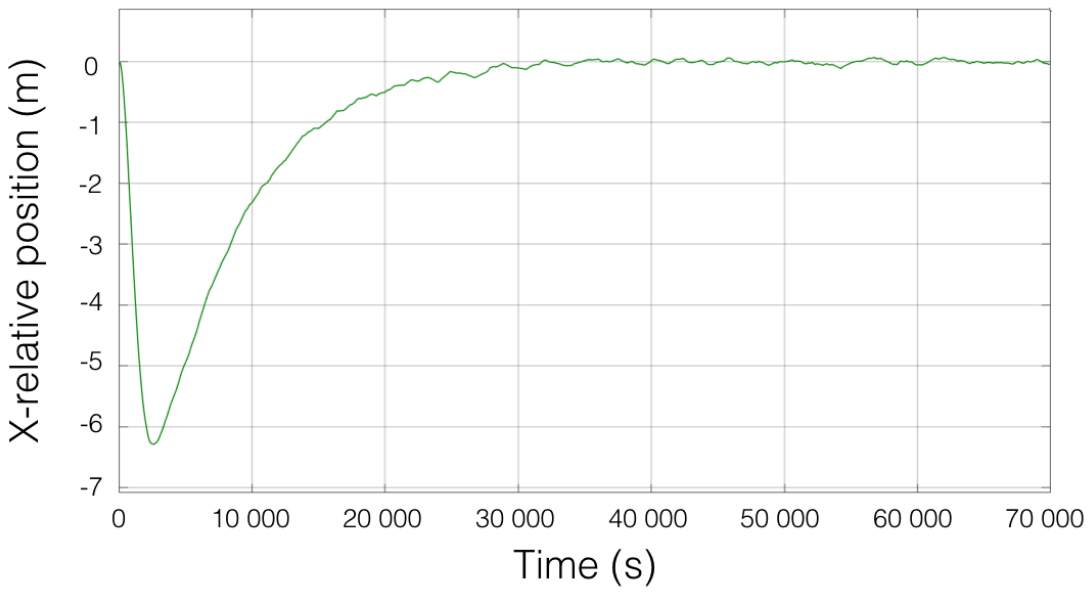

Figure 5.4: X-relative position over time using the GPS for the second closing approach

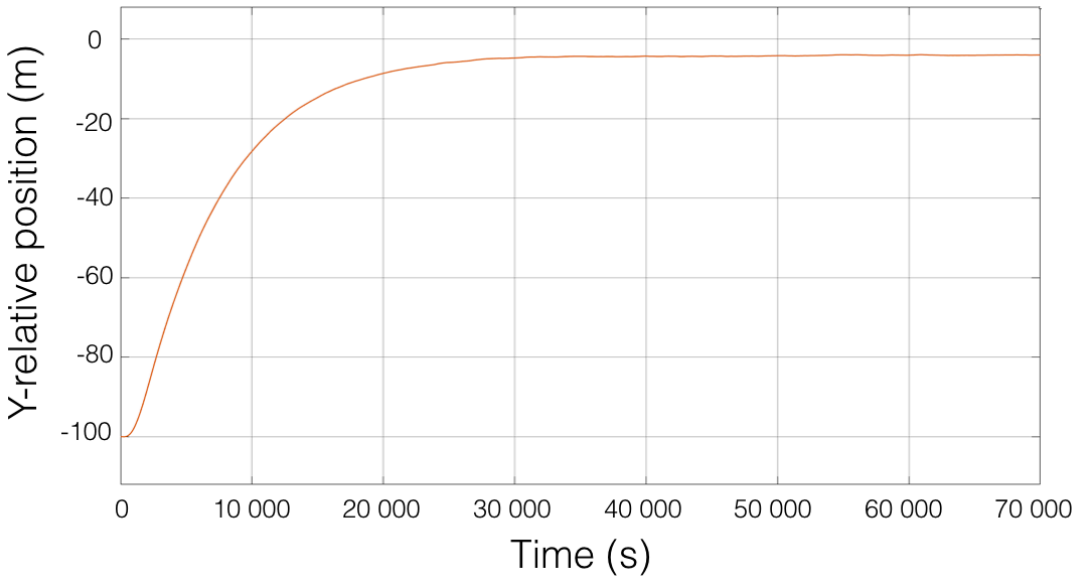

Figure 5.5: Y-relative position over time using the GPS for the second closing approach

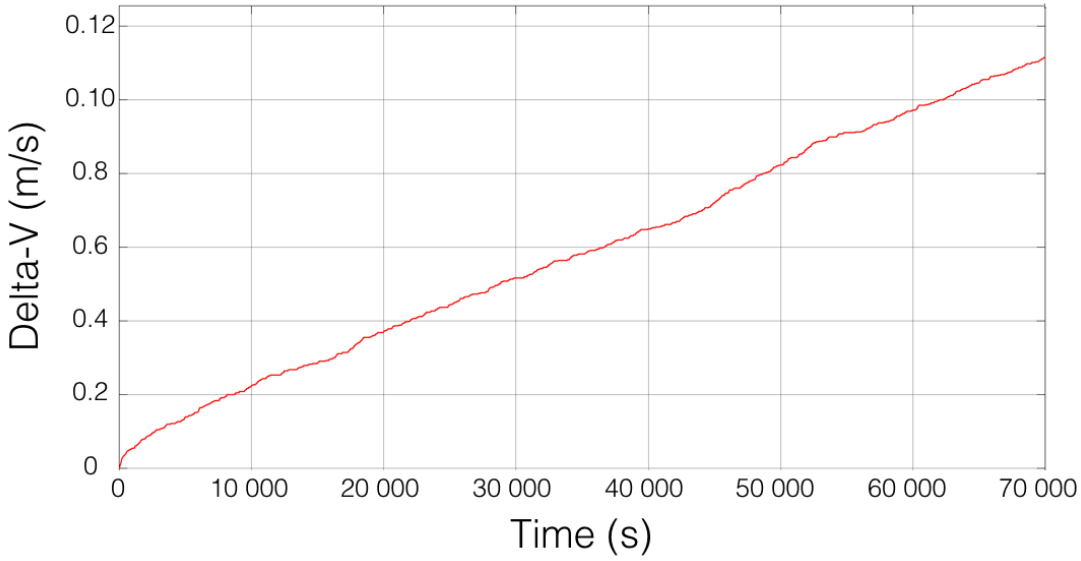

Figure 5.6: Delta-V spent during the second closing approach

From Figure 5.1, Figure 5.2, Figure 5.4 and Figure 5.5, we see that the relative position converges in approximately 17 hours for phase 1 and 11 hours for phase 2 with a final accuracy around +/- 20 cm around the target position [0; -4m; 0]. This distance is close enough to switch to a more accurate proximity sensor. Assuming that the total duration of phases 1 and 2 is about 28 hours, the total delta-V is about 0.6 m/s, which corresponds to the total propellant mass 0.018 kg. For bigger initial distance separations, this delta-V would increase up to 3 m/s for phase 1 and 2 up to 30 km separation distance. This delta-V can be traded off with the convergence speed.

5.3 Final approach ΔV and accuracy results

Once the satellite is close enough after the first approach maneuver, highly accurate proximity sensors can be used to determine the relative position. The chaser satellite is then navigated from a few meters separation distance (4 m along the y axis) to a few centimeters (60 cm along the y axis) from the target using proximity sensors. The starting point is at [0 m; -4 m; 0 m]. The resulting X, Y relative position of the chaser is shown in Figure 5.7 and Figure 5.8. The delta-V over time is shown in Figure 5.9.

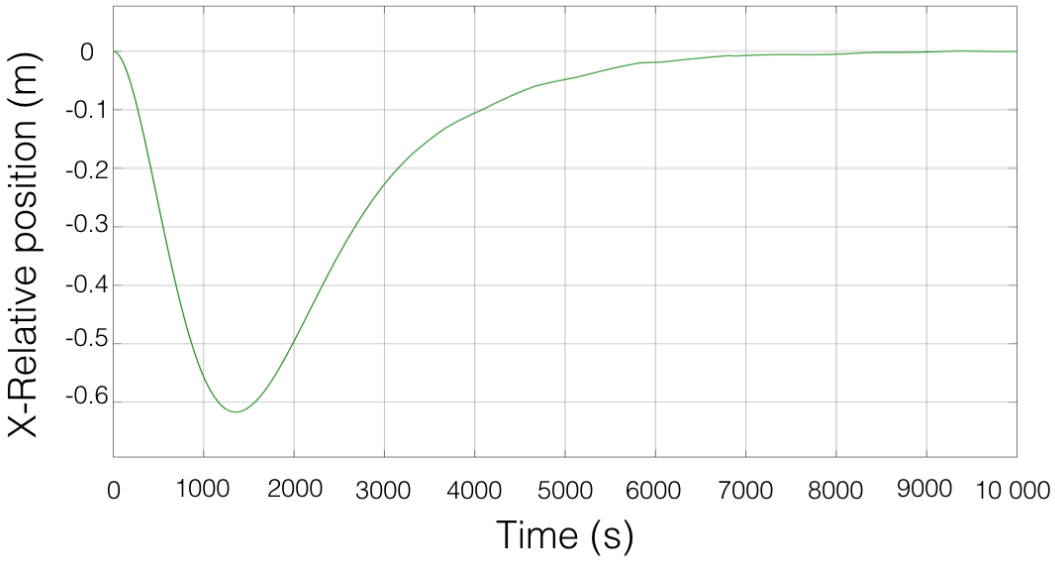

Figure 5.7: X-relative position over time using the proximity sensors for the final approach

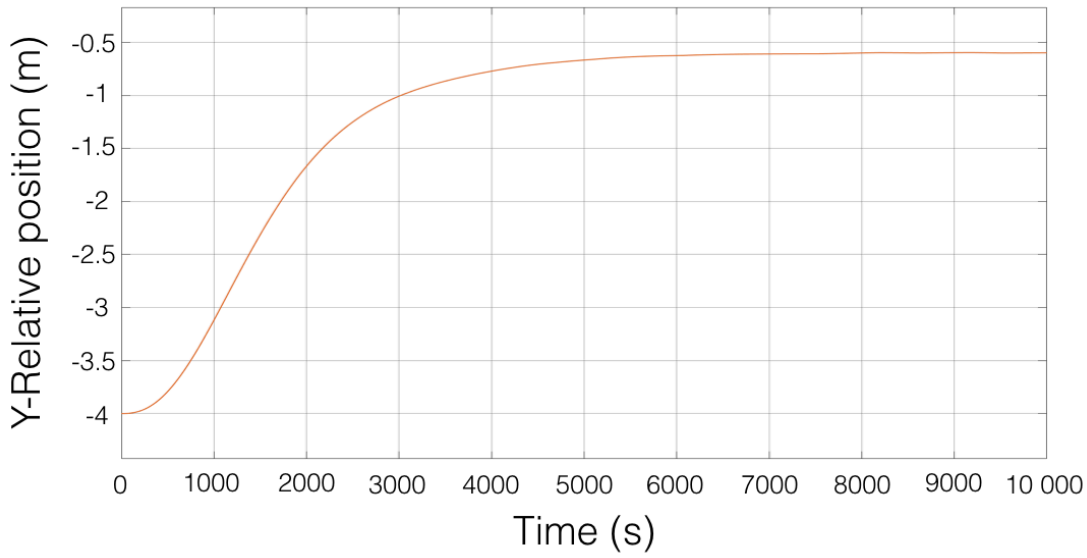

Figure 5.8: Y-relative position over time using the proximity sensors for the final approach

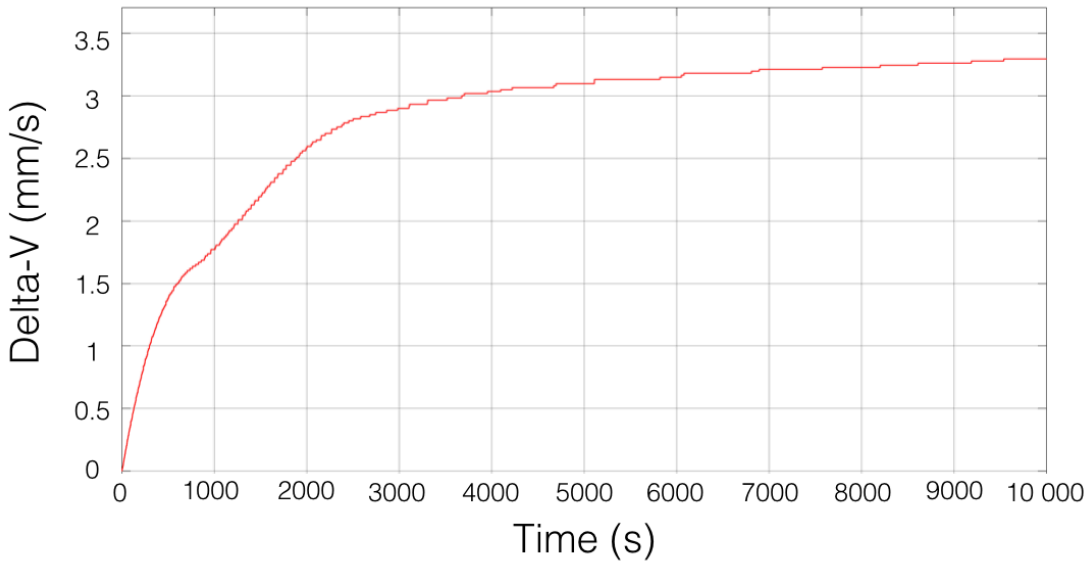

Figure 5.9: Delta-V spent during the final approach approach

The results show that the satellite is then able to stay within a range of the order of +/- 1 cm around the target, which is enough for the robotic arms to deploy and dock. Assuming that the total duration of the final approach phase is about 2.5 hours, the total delta-V is about 3.5 mm/s, which corresponds to a propellant mass 0.11 g.

CHAPTER 6 BENEFITS OF USING ROBOTIC ARM

6.1 Station keeping scenario

Besides its advantages of in-space assembly applications, docking safety and high accuracy relative position determination and control for example, the use of a robotic arm will also help to significantly reduce the delta V spent for station keeping as compared to traditional "armless" formation flying missions. In order to estimate the amount of fuel spent this mission could save, a simple model has been created. It compares the (A) propellant needed to keep the relative position of 2 satellites (without robotic arm) using thrusters and (B) propellant needed to keep the attitude of a thin bar (arm) with a satellite on each end using thrusters. The propellant in (A) is used to cancel the difference of orbital velocity, and the propellant in (B) is used to cancel the gravity gradient torque. In both situations, perfect sensors and actuators are assumed. The real fuel savings will depend on the components selected and the number of satellites considered, this investigation gives a first order minimum fuel savings estimation.

With these assumptions, the method to compute the fuel spent for (A) was based in the Clohessy-Wiltshire equations (Equation 4.8, Equation 4.9 and Equation 4.10) where the requirement for station keeping was to set both acceleration and velocity to 0.

$$0 = 3n^2x + u_x + d_x \tag{6.1}$$

$$0 = u_y + d_y \tag{6.2}$$

$$0 = -n^2 z + u_z + d_z \tag{6.3}$$

For this problem, the relative drag is insignificant since the chaser and the target have the same velocity and altitude (i.e. residual atmosphere density). Moreover, when the two satellites are closer than 1 meter, the differential J2 disturbance is always at least 1000 times less than the nominal control. Therefore, the control needed to keep the chaser without robotic arm can accurately be approximated as:

$$\boldsymbol{u} = n^2[-3x\ 0\ z]^T \tag{6.4}$$

For case (B), the robotic arm keeps the two satellite together. Nonetheless, the structure has to counteract the gravity gradient effect, which torque around the Y-axis is found to be:

$$T_G = -\frac{3}{4} m \frac{\mu}{R} l^2 \sin(2\alpha) \tag{6.5}$$

Where m is the mass of the chaser, μ is the gravitational parameter of the Earth, R is the radius of the target circular orbit, l is the length of the robotic arms and α is the angle of the bar with respect to the local frame. The angle grows positively from Z to X and is 0 when the bar is in the X-direction. The two configurations along the X-direction are two stable equilibrium positions whereas the two equilibrium positions

along the Z-direction are not stable. In the Z-X plane the torque can be expressed with respect to the X and Z-coordinates in order to compare the fuel consumption between (A) and (B) using $lcos(\alpha) = x$ and $lsin(\alpha) = z$:

$$T_G = -\frac{3}{2} m \frac{\mu}{R} xz \tag{6.6}$$

The following heat map in Figure 6.1 shows the delta V spent daily with respect to the relative position of the two satellites in the Z-X plan. Y is set to zero since the Y-axis (along the velocity direction) has a very low influence in this problem.

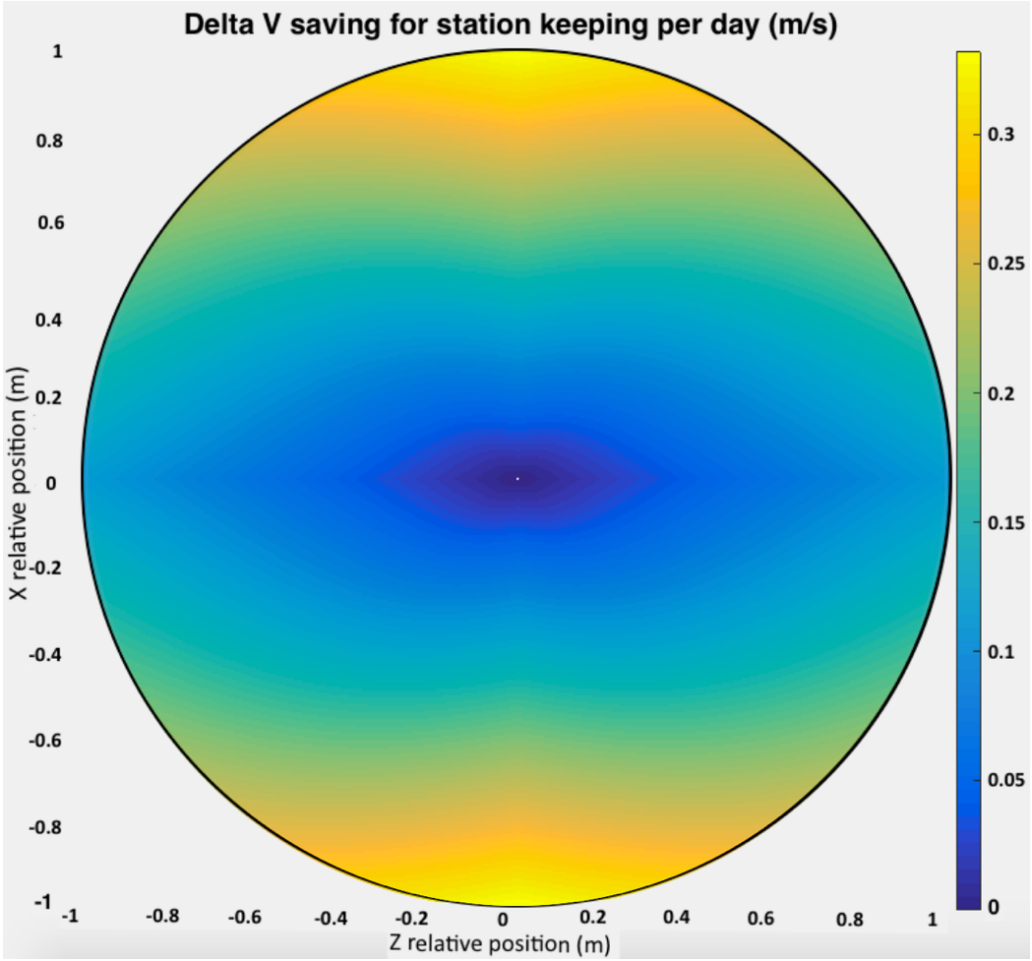

Figure 6.1: Daily delta-V savings for different configuration in the Z-X plane

In (A), the consumption of propellant increases with the increase in distance in either direction, however, fuel is spent threefold in the case of sole increments in X-coordinate (maximum velocity difference) than in Z-coordinate. Here, (B) consumes no propellant when X = 0 or Z = 0 (no gravity gradient effect) and the consumption of propellant is highest when X = Z (45 deg configuration).

Subtracting (A) - (B) yields to the result that the saving is the largest when Z = 0 and smallest when X = 0 given the same arm length because the effects of (A) is larger than

that of (B). In the largest saving case (Z = 0), we can save up to about 110m/s of delta-V per year, which corresponds to about 3.5 kg of propellant with a 40 s Isp and 12 kg spacecraft.

6.2 Reconfiguration scenario

In addition to station-keeping scenario, another fuel savings analysis was carried out to quantify the benefit of using the robotic arm. This is in the case of reconfiguration maneuvers. It compares the (A) propellant needed to move the chaser from one relative position to another (without robotic arm) using thrusters and (B) the change of the attitude of a thin bar (arm) with a satellite at each end using reaction wheels or robotic actuators (no fuel spent). The manoeuver (A) relies on the 2 impulses control method computed from the transition matrix of the Clohessy-Wilshire equations, which assumes instantaneous impulses and does not take into account the collision avoidance issue. It is therefore a minimum fuel consumption estimation. Both (A) and (B) assume perfect sensors and actuators.

From the linearized set of equations derived in Chapter 4 where no control or disturbances are applied, any state at time t can be found according to its previous state at time 0:

$$\boldsymbol{x}(t) = \Phi(t)\boldsymbol{x}(0) \tag{6.7}$$

Where

$$\boldsymbol{x} = \begin{bmatrix} x \\ y \\ z \\ \dot{x} \\ \dot{y} \\ \dot{z} \end{bmatrix} \tag{6.8}$$

$$\Phi(\mathrm{t}) = \begin{bmatrix} 4-3\cos(nt) & 0 & 0 & \frac{\sin(nt)}{n} & \frac{2}{n}(1-\cos(nt)) & 0 \\ 6(\sin(nt)-nt) & 1 & 0 & \frac{2}{n}(\cos(nt)-1) & \frac{4\sin(nt)-3nt}{n} & 0 \\ 0 & 0 & \cos(nt) & 0 & 0 & \frac{\sin(nt)}{n} \\ 3n\sin(nt) & 0 & 0 & \cos(nt) & 2\sin(nt) & 0 \\ 6n(\cos(nt)-1) & 0 & 0 & -2\sin(nt) & 4\cos(nt)-3 & 0 \\ 0 & 0 & -n\sin(nt) & 0 & 0 & \cos(nt) \end{bmatrix} \tag{6.9}$$

Equation 6.7 gives 6 independent equations between the initial and final relative positions and velocities (12 variables) of the chaser with respect to its target. By fixing the initial and final positions (6 variables) we are left with 6 unknown velocity variables that can be derived by solving the 6 equations system in Equation 6.7. The initial ones represent the first impulse to apply whereas the final ones represent the opposite of the final impulse needed in order to stop spacecraft. This method can be applied to any reconfiguration possible.

In order to estimate the amount of delta-V the robotic arms can save in a potential realistic interferometry mission, the following heat maps shows an example of a representative reconfiguration scenario. Starting from a defined initial position, Figure

6.2 represents the delta-V needed for the chaser to reach its corresponding final position in the Y-Z plane for the two impulses maneuvers. It is compared to the situation where no propellant is needed for the robotic arms since they allow to reconfigure the formation to any relative positions included in the half circle they can reach (here for example, any Y relative positions and only positive Z relative positions). The reconfiguration transfer time has been set to 4 minutes, a reasonable time to compare with the robotic reconfiguration solution.

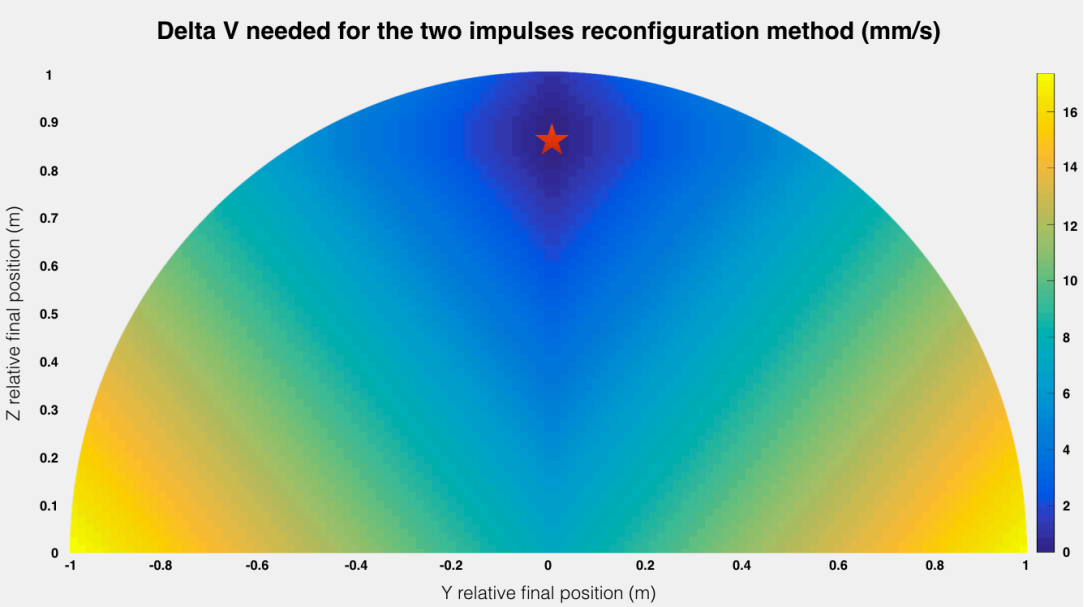

Figure 6.2: Example of delta-V savings for the reconfiguration maneuvers in the half circle reachable by the robotic arms. Here the initial condition is the red star with coordinates [0 cm ; 0 cm ; 86 cm]

In (A), the consumption of propellant increases with the increase in distance in either direction. In the considered scenario, maneuvers along the chaser-target axis in (B) are especially simple since it only consists on reducing the length of the robotic arm. This kind of maneuvers are particularly suitable for interferometry missions where precise

relative distance changes are required. An example is shown in Figure 6.3 where an interferometry formation of four SmallSats is changing the separation distances between each spacecraft:

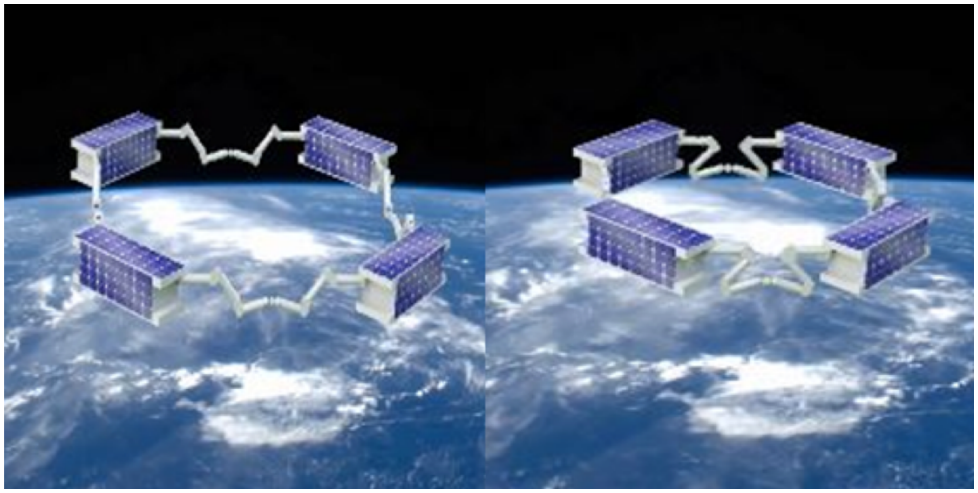

Figure 6.3: Example of a reconfiguration scenario, the formation is being changed for interferometry purposes, from JPL

According to the sizes of the 6U CubeSats and the length of the robotic arms considered, it corresponds to a reconfiguration of each satellite distance from the formation center of gravity from maximum 86 cm to minimum 21 cm. Using the method described above applied to a formation relying in the Y-Z plane with two spacecraft along the Y-axis and the two others along the Z-axis, the fuel savings have been estimated. Under all the assumptions mentioned, the following Figure 6.4 represents the total amount of delta-V needed to reconfigure this formation from its minimum to its maximum extension with respect to the reconfiguration time (from 30 seconds to 10 minutes here).

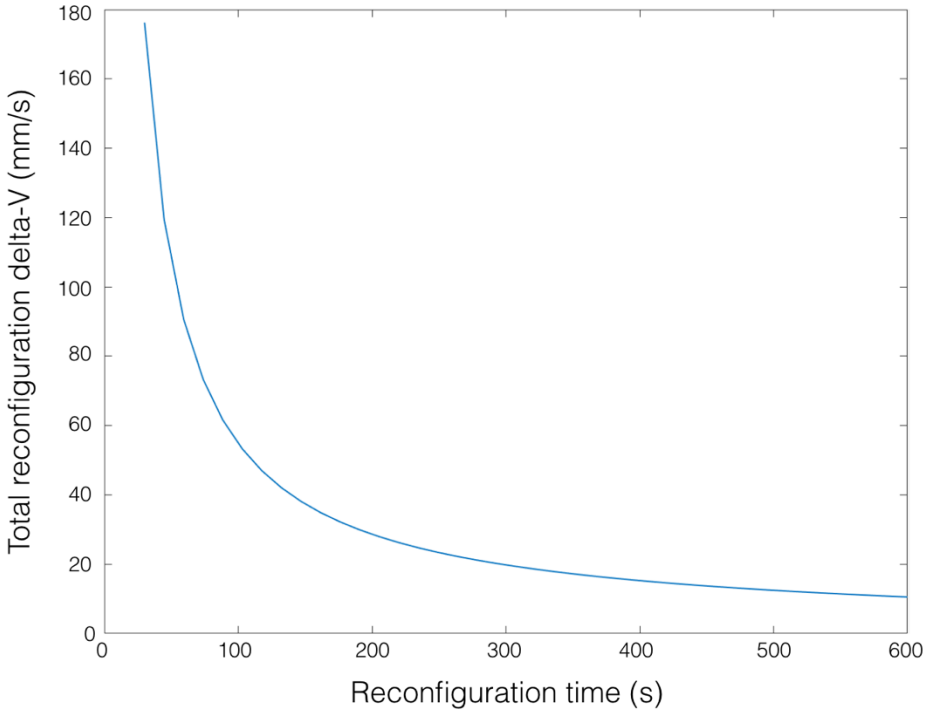

Figure 6.4: Total delta-V spent to change the four satellites interferometry formation with respect to the reconfiguration time

Over the mission lifetime, and depending on how frequent these reconfigurations are needed to occur, the amount of delta-V savings can be significant. It can be scalded to the size of the formation.

CHAPTER 7 CONCLUSION

This research developed a concept of SmallSat cluster connected with robotic arms, aiming to enable a broad range of scientific and engineering applications with a low-cost and reconfigurable design. Multiple SmallSats are operated in a cluster, and the robotic arms on each SmallSat can perform docking and rendezvous between the SmallSats as well as holding and reconfiguring the formation to meet the demands of scientific missions. An example of a realistic concept of operations for the launch, deployment and docking was presented in order to determine the constraints of the mission. In parallel, JPL developed a miniaturized robotic arm able to fit in a 0.5 CubeSat unit and enabled the docking phase with the help of their unique end effector design. The selection of the satellite bus components was then based on their performances and flight heritage. Under all these constraints raised by the selected sensor and actuator features and mission expectations, a realistic simulation and a control law was created in order to assess the feasibility of such a challenging mission. The final results revealed that the performances of the considered satellites were in compliance with the requirements for the robotic arms to dock.

In order to conclude this mission design investigations, future work will need to be done about the attitude control of the spacecraft during the rendezvous and docking phases, especially taking into account the interaction of the spacecraft physical body with its performances during the final approach. Another crucial study will need to be carried out about the multi-body dynamics of the final SmallSat cluster linked with their robotic arms to understand its precise attitude control.

CHAPTER 8 PUBLICATION AND CONFERENCES

The research carried out thorough this Thesis added to the work done about the robotic arms by JPL has been published and presented to the IEEE Aerospace conference (9 March 2017):

- R. McCormick et al., “Development of Miniature Robotic Manipulators to Enable SmallSat Clusters,” in IEEE Aerospace Conf., Big Sky, Montana, 2017.

We plan to publish an updated journal paper including all the recent work done for Astra Astronomica in the coming months.

REFERENCES

[1] R. McCormick et al., “Development of Miniature Robotic Manipulators to Enable SmallSat Clusters,” in IEEE Aerospace Conf., Big Sky, Montana, 2017.

[2] Dunbar, Brian. "SmallSat Proximity Operations Demonstration (CPOD)."NASA. NASA, n.d. Web. 28 July 2016.

[3] Pellegrino, Sergio. "AAReST Overview." -. CalTech, n.d. Web. 25 July 2016.

[4] J. Hamel, “Autonomous Guidance and Control of Earth-Orbiting Formation Flying Spacecraft”, Université de Sherbrooke, Sherbrooke, Canada, 2007.

[5] C. Kluever, "Feedback Control for Spacecraft Rendezvous and Docking," Journal of Guidance, Control, and Dynamics, vol. 22, no. 4, pp. 609-611, Aug. 1999.

[6] S. Wu, W. Zhou, S. Tan and G. Wu, "Robust H∞ Control for Spacecraft Rendezvous with a Noncooperative Target," The Scientific World Journal, vol. 2013, pp. 1-7, Apr. 2013.

[7] Z. Zhou, "Trajectory Control of Rendezvous with Maneuver Target Spacecraft," in AIAA/AAS Astrodynamics Specialist Conf., Mineapolis, Minnesota, Aug. 2012.

[8] P. A. Felisiak, K. S. Sibilski, W. A. Wroblewski and J. Z. Sasiadek, "Spacecraft Rendezvous in Elliptical Orbit using Nonlinear Model Predictive Control," in AIAA Guidance, Navigation, and Control Conf., National Harbor, Maryland, Jan. 2014.

[9] D. Morgan, S. Chung and F. Hadaegh, "Model Predictive Control of Swarms of Spacecraft Using Sequential Convex Programming," Journal of Guidance, Control, and Dynamics, vol. 37, no. 6, pp. 1725-1740, Dec. 2014.

[10] E. Lightsey "SmallSat Formation Flying," Workshop on SmallSat-based Low Frequency Radio Astronomy Missions, Pasadena, CA, 2012.

[11] M. D'Errico, Distributed Space Missions for Earth System Monitoring, McGraw-Hill, 2013.

[12] D. Maessen, "Autonomous Relative Navigation for Small Spacecraft," PhD Thesis, TU Delft, 2014.

[13] K. Ui, S. Matunaga, S. Satori and T. Ishikawa, "Microgravity Experiments of Nano-Satellite Docking Mechanism for Final Rendezvous Approach and Docking Phase," Tokyo Inst. of Tech., Tokyo Metropolitan Col. of Aero. Tech. and Hokkaido Inst. Tech, Tokyo, Jaoan, Mar. 2005.

[14] W. Xu, B. Liang, C. Li and Y. Xu, "Autonomous rendezvous and robotic capturing of non-cooperative target in space," Robotica, vol. 28, no. 05, pp 705-718, Sep. 2008.

[15] I. Kawano, M. Mokuno, T. Kasai and T. Suzuki, "Result of Autonomous Rendezvous Docking Experiment of Engineering Test Satellite-VII," National Space Development Agency, Tsukuba, Ibaraki, Japan, Feb. 2001.

[16] F. Boyer, V. Lebastard, C. Chevallereau, S. Mintchev and C. Stefanini, "Underwater navigation on passive electric sense: new perspectives for underwater docking," CNRS, Nantes, France, Dec. 2014

[17] C. P. Bridges, B. Taylor, N. Horri, C. I. Underwood, S Kenyon, J. Barrera-Ars, L. Pryce and R. Bird, "STRaND-2: Visual Inspection, Proximity Operation & Nanosatellite Docking," University of Surrey and Surrey Satellite Technology Ltd., Guildford, Surrey, UK, May 2012.

[18] C. Underwood, S. Pellegrino, V. J. Lappas, C. p. Bridges and J. Baker, ""Using SmallSat/micro-satellite technology to demonstrate the Autonomous Assembly of a Reconfigurable Space Telescope (AAReST)," Surrey Space Center, Univ. of Surrey and Caltech/JPL, Guildford and Pasadena, Surreu and CA, UK and USA, Apr. 2015.

[19] D. Selva and D. Krejci, "A Survey and Assessment of the Capabilities of SmallSats for Earth Observation," Acta Astronautica, Vol. 74, pp. 50-68, 2012.

[20] S. Spangelo, M. Bennett, D. Meinzer, A. Klesh, J. Arlas and J. Cutler, "Design and implementation of the GPS subsystem for the Radio Aurora eXplorer", Acta Astronautica, vol. 87, pp. 127-138, Jan. 2013.

[21] GomSpace. NovAtel OEM615 Dual-Frequency GPS. Aalborg East, Denmark: GomSpace ApS, n.d. GomSpace ApS, Web. 22 Nov. 2016 < https://gomspace.com/UserFiles/Subsystems/datasheet/gs-ds-novatel-gpsoem615-10.pdf >

[22] SoftKinetic. DS525. Korea: SoftKinetic, n.d. SoftKinetic. Web. < https://www.softkinetic.com/Portals/0/Documents/PDF/WEB_20131230_SK_DS525_Datasheet_V2.1.pdf >

[23] Vacco. Reaction Control Propulsion Module. South El Monte, CA: Vacco, n.d. ESCO Technologies, Inc. Web. < http://www.cubesat-propulsion.com/wp-content/uploads/2015/10/Reaction-control-propulsion-module.pdf >

[24] Blue Canyon Technologies. XACT: High-Performance Attitude Determination for SmallSats. N.p.: Blue Canyon Technologies, n.d. Blue Canyon Technologies. Web.

[25] Space Micro. Proton200k Lite Processor Board. San Diego: Space Micro, n.d. Space Micro. Web.

[26] Innovative Solutions In Space. TRXUV VHF/UHF Transceiver. Delft, The Netherlands: Innovative Solutions In Space, n.d. Innovative Solutions In Space. Web.

[27] Endurosat. S-Band Patch Antenna Type I. N.p.: Endurosat, n.d. Endurosat, 2016. Web. < https://www.endurosat.com/capabilities-and-products/s-band-patch-antenna/ >.

[28] "Products." Clyde Space. Clyde Space, n.d. Web. 15 Aug. 2016.

[29] Mirko Leomanni, Stephen Gabriel and Eric Rogers, “The Applicability of Pulsed Plasma Thrusters to Rendezvous and Docking of Cubesats”, International Electric Propulsion Conference, Washington, D.C., USA, Oct 2013

[30] H. Djojodihardjo, "INFLUENCE OF THE EARTH’S DOMINANT OBLATENESS PARAMETER ON THE LOW FORMATION ORBITS OF MICRO-SATELLITES", International Journal of Automotive and Mechanical Engineering, vol. 9, pp. 1802-1819, 2014.

[31] Gill, Eberhard, Oliver Montenbruck, and Simone D'Amico. "Autonomous Formation Flying For The PRISMA Mission". Journal of Spacecraft and Rockets 44.3 (2007): 671-681